JUSTC

Article

http://justc.ustc.edu.cn

Received: October 10, 2025; Accepted: March 16, 2026

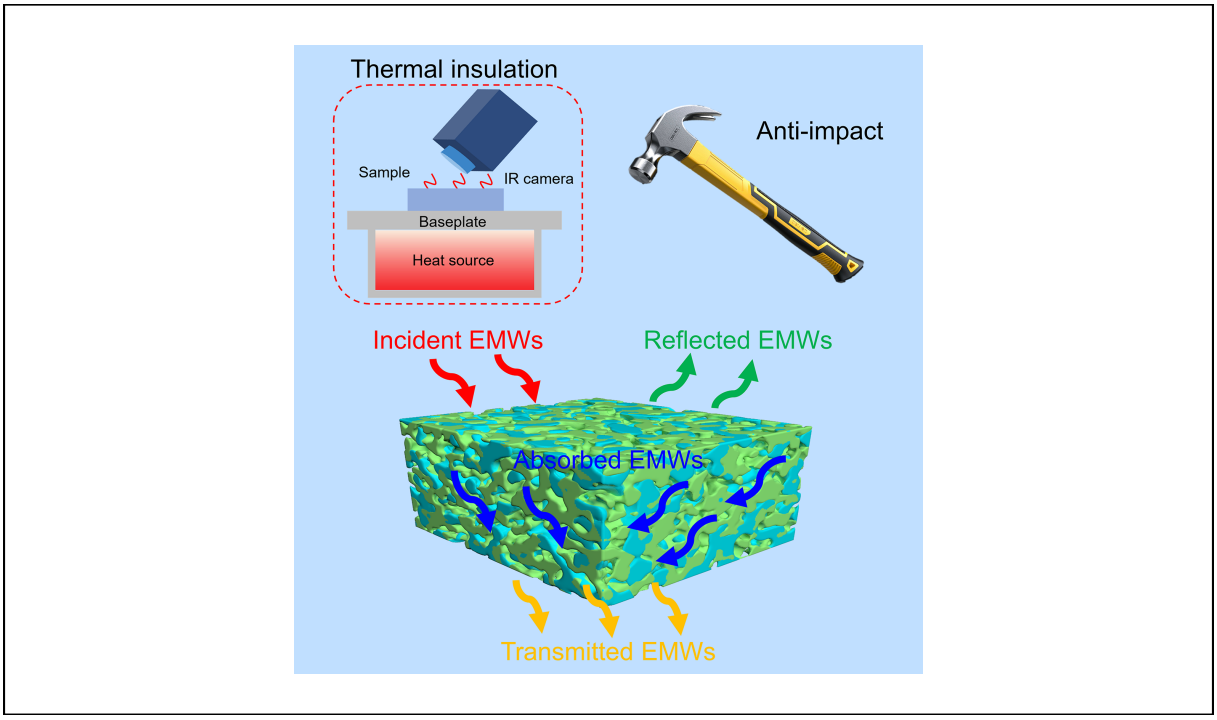
Shear Stiffening-Reinforced Conductive Nickel Metal Composite Foam for Impact-Thermal Protection and High-Performance Electromagnetic Shielding

Tongxin Nie[1], Min Sang[1] ✉, Shuai Liu[1], Yucheng Pan[1], Jianpeng Wu[1], Shilong Duan[1], Zhentao Zhang[1], and Xinglong Gong[1,2] ✉

[1]*CAS Key Laboratory of Mechanical Behavior and Design of Materials, Department of Modern Mechanics, University of Science and Technology of China, Hefei, Anhui 230027, P. R. China;*
[2]*State Key Laboratory of Fire Science, University of Science and Technology of China, 96 Jinzhai Road, Hefei, Anhui, 230026, P. R. China*

✉Correspondence: Min Sang, sm019050@ustc.edu.cn; Xinglong Gong, gongxl@ustc.edu.cn
© 2026 The Author(s). This is an open access article under the CC BY-NC-ND 4.0 license (http://creativecommons.org/licenses/by-nc-nd/4.0/).

Graphical abstract



This study fabricated a conductive Ni-coated composite foam with dispersed SSG, showing excellent impact-thermal protection and electromagnetic shielding.

Public summary

■ The SSG/Ni composite foam showed obvious shear stiffening behavior and enhanced mechanical strength.

■ The SSG/Ni composite foam exhibited excellent impact resistant and energy absorption performance.

■ The SSG/Ni composite foam presented ideal thermal insulation and protection property.

■ The SSG/Ni composite foam possessed superior electromagnetic shielding effectiveness.

Citation: Nie T X, Sang M, Liu S, et al. Shear Stiffening-Reinforced Conductive Nickel Metal Composite Foam for Impact-Thermal Protection and High-Performance Electromagnetic Shielding. *JUSTC*, **2026**, 56(0): . CSTR: 32290.14.JUSTC-2025-0103. DOI: 10.52396/JUSTC-2025-0103

JUSTC

Article

http://justc.ustc.edu.cn

Received: October 10, 2025; Accepted: March 16, 2026

Shear Stiffening-Reinforced Conductive Nickel Metal Composite Foam for Impact-Thermal Protection and High-Performance Electromagnetic Shielding

Tongxin Nie[1], Min Sang[1] ✉, Shuai Liu[1], Yucheng Pan[1], Jianpeng Wu[1], Shilong Duan[1], Zhentao Zhang[1], and Xinglong Gong[1,2] ✉

[1]*CAS Key Laboratory of Mechanical Behavior and Design of Materials, Department of Modern Mechanics, University of Science and Technology of China, Hefei, Anhui 230027, P. R. China;*
[2]*State Key Laboratory of Fire Science, University of Science and Technology of China, 96 Jinzhai Road, Hefei, Anhui, 230026, P. R. China*

✉Correspondence: Min Sang, sm019050@ustc.edu.cn; Xinglong Gong, gongxl@ustc.edu.cn
© 2026 The Author(s). This is an open access article under the CC BY-NC-ND 4.0 license (http://creativecommons.org/licenses/by-nc-nd/4.0/).

Cite This: *JUSTC*, **2026**, 56(X): (11pp) Read Online SI Supporting Information

Abstract: As the most common hazards in daily life, impact-thermal shock and electromagnetic radiation inevitably negatively affect national security and economic development. The development of high-performance and multifunctional protective materials is highly important since a single protective material is no longer sufficient to meet the demands of complex and extreme environments. In this work, a multi-protective composite material with high-performance impact resistance, thermal insulation and electromagnetic shielding was developed by integrating shear stiffening gel (SSG) with conductive Ni-coated foam. The conductive Ni-coated foam served as the conductive component and heat insulation medium, while the SSG was used as the reinforcing phase to further enhance its mechanical performance. The resulting SSG/Ni composite foam effectively attenuated external impact forces, and the absorption rate of the impact energy exceeded 90%. Owing to the low thermal conductivity of the conductive Ni-coated foam (0.039 W m^{-1} K^{-1}), the SSG/Ni composite foam exhibited excellent thermal insulation properties over a wide temperature range from 50 to 200 °C. At a thickness of 5 mm, the SSG/Ni composite foam showed superior electromagnetic shielding performance, with a maximum shielding effectiveness of 80 dB, which far exceeded the commercial and industrial requirements. This work provides a feasible strategy for the development of next-generation multimodal functional protective materials.

Keywords: Conductive foam; Shear stiffening; Thermal insulation; Electromagnetic shielding; Multiple protections

CLC number: **Document code:** A

1 Introduction

Safety protection has always been a major social issue that humanity has had to confront throughout history [1]. Violent collisions and dynamic impacts in various extreme environments (such as car accidents, air turbulence, and wars) have posed significant threats to human life; thus, the development of impact-resistant protective materials has become the foundation of human engineering technology, playing a crucial role in protecting the human body, precision equipment, and spacecraft [2]. Shear-stiffening materials, as a new type of impact-resistant protective material, have emerged in fields such as vibration control, impact protection, and flexible wearables [3,4]. Shear-stiffening material is an intelligent material that is sensitive to strain rates. Owing to this unique strain rate enhancement effect, shear-stiffening materials can rapidly harden when subjected to impact, effectively absorbing and dispersing external energy to achieve outstanding protective performance [5]. Therefore, shear-stiffening materials have demonstrated broad application prospects in fields such as personal protection, equipment protection, and military defense; these materials provide high-level protection for various types of equipment and have become highly promising advanced materials [6–8]. Inspired by annular structure, Li et al. embedded rigid epoxy resin into a flexible annular shear-stiffening rubber-based skeleton to develop an annular shear-hardening rubber-based smart material. This soft–hard coupling design can not only adjust its mechanical properties according to complex working conditions to provide better protection but also features shape-programming capabilities, enabling it to adapt to different protection requirements [9].

With the continuous development of science and technology, the widespread application of electronic devices and wireless communication technologies has made the problem of electromagnetic interference (EMI) increasingly prominent [10,11]. Electromagnetic interference can not only significantly affect the normal operation and function of electronic devices but also pose a serious threat to human health [12,13]. Therefore, developing electromagnetic shielding materials to reduce the interference of electromagnetic radiation has become an important issue that needs to be urgently addressed in the current 5G and 6G era. Generally, the electrical conductivity of a material is the key factor in determining its

CSTR: 32290.14.JUSTC-2025-0103
DOI: 10.52396/JUSTC-2025-0103
JUSTC, **2026**, 56(X):

electromagnetic shielding performance; metallic materials such as copper, aluminum, and silver are widely used as shielding materials because of their excellent electrical conductivity [14–16]. However, metallic materials have high densities and poor corrosion resistance, which limits their further application. Recently, conductive nickel-coated foam has garnered increasing interest as an effective material for advanced electromagnetic shielding applications because of its unique three-dimensional porous structure and superior electrical conductivity [17–19]. Its lightweight nature also makes it particularly attractive for applications where weight reduction is essential. Nickel metal-based foam is usually developed by coating metallic nickel onto a three-dimensional polymer foam via chemical vapor deposition method; thus, its mechanical properties are relatively poor. To address this, combining SSG with conductive nickel-coated foam not only enhances the mechanical properties of the nickel-coated foam itself but also endows the material with excellent impact resistance and electromagnetic shielding capabilities.

Apart from impact resistance and electromagnetic shielding, the integration and optimization of thermal insulation have attracted increasing interest [20,21]. Similar to electromagnetic radiation interference, thermal shock loading not only affects the functionality of electronic devices but also causes thermal damage to the human body [22,23]. Therefore, developing high-efficiency thermal protection materials is crucial for applications in personal and engineering protection. According to heat transfer theory, the thermal conductivity of gases is usually lower than that of solids [24,25]. Owing to the presence of a large volume of trapped air, porous materials possess excellent thermal insulation properties and are widely used in building insulation, aerospace, and industrial equipment [26]. Furthermore, the porous structure creates a tortuous heat transfer path, requiring multiple directional changes through the solid framework and the gases within the pores, thereby increasing the thermal resistance and reducing the thermal conductivity [27]. For example, Liu et al. proposed a host–guest structural composite material composed of viscoelastic polyborosiloxane (PBS) dispersed in a porous polyimide (PI) matrix. Owing to the low thermal conductivity of the porous polyimide, PI-PBS exhibits excellent thermal insulation performance over a wide temperature range (approximately 80–300 °C) [28]. However, effectively integrating energy dissipation, thermal insulation, and electromagnetic shielding remains a significant challenge owing to the complexity of structural design.

Herein, a simple method was developed to fabricate a multimodal protective structural SSG/Ni composite possessing excellent impact resistance, thermal insulation, and electromagnetic shielding capabilities by combining SSG with conductive Ni-coated foam. Owing to the rate-dependent property of the SSG, the resulting SSG/Ni composite foam exhibited an effective ability to attenuate impact forces under external mechanical impacts. The spatial distribution of the impact force was demonstrated via a distinct mechanodiscoloration method, which provides compelling evidence for the protective mechanism. Interestingly, the porous structure of the Ni-coated foam endows the composite material with excellent thermal insulation properties, effectively blocking heat transfer and providing thermal protection. Infrared thermal imaging experiments further revealed that the excellent thermal insulation performance enables the SSG/Ni composite foam to be effectively applied in the field of infrared thermal camouflage. More importantly, the 3D conductive structure of the conductive nickel foam successfully facilitates the reflection, absorption, and multiple internal reflections of electromagnetic radiation, effectively shielding against electromagnetic waves. This functional material, which integrates impact protection, thermal protection, and electromagnetic wave protection has the potential to become the preferred candidate for the next generation of multimodal protective materials to meet the demands of various extreme and complex environments.

2 Materials and Methods

2.1 Materials

Hydroxyl silicone oil, boric acid, octanoic acid, and ethanol were purchased from Sinopharm Chemical Reagent Co., Ltd., Shanghai, China. Conductive Ni foam was a commercially available product in China. All reagents were used without further purification, and distilled water was used throughout the experiments.

2.2 Preparation of Shear Stiffening Gel (SSG)

The SSG was prepared according to our previous report [29]. Briefly, the hydroxyl silicone oil and boric acid were blended at a mass ratio of 20:1 and then stirred and heated at 180 °C for 2 h in an oven. After the boric acid was allowed to react completely, 250 μL of octanoic acid (per 100 g of hydroxyl silicone oil) was added to the mixture, followed by heating and stirring for another 30 min. Finally, the resulting product was cooled to room temperature, and the SSG was obtained.

2.3 Fabrication of Conductive SSG/Ni Composite Foam

A facile ultrasonic-assisted infiltration–drying approach was adopted to fabricate the conductive SSG/Ni composite foam. First, the prepared SSG was dissolved in ethanol to obtain a uniformly dispersed SSG/ethanol solution (800 mg/mL). Subsequently, the commercially available conductive Ni foams with different thicknesses were immersed in the SSG/ethanol solution and subjected to ultrasonication (200 W) for 120 min to facilitate the infiltration of SSG into the porous networks. Afterwards, the infiltrated foams were dried in an oven at 60 °C until the ethanol was completely removed. Finally, conductive SSG/Ni composite foams with different thicknesses were obtained.

2.4 Characterization

The microstructures of the conductive Ni and SSG/Ni composite foams were characterized by scanning electron microscopy (SEM, Sirion 200) equipped with an energy-dispersive spectroscopy (EDS) system. The compressive and tensile properties were tested using a universal electronic material testing machine (MTS, Criterion Model 43, MTS Co., Ltd., China). The impact resistance was evaluated using an automatic drop hammer testing system (ZCJ-1302-A, MTS Co., Ltd., China). The thermal insulation property was assessed by

CSTR: 32290.14.JUSTC-2025-0103
DOI: 10.52396/JUSTC-2025-0103
JUSTC, **2026**, 56(X):

recording the temperature variations under a heating plate using a multichannel thermocouple (DT-3891G, Shenzhen Everbest Machinery Industry Co., Ltd., China). The corresponding infrared radiation (IR) thermal images were recorded by an infrared camera (ImageIR 8300, InfraTec, Germany). The thermal conductivity was measured on a laser thermal conductivity meter (LFA457, Netzsch, Germany) via the HotDisk method. The electromagnetic interference shielding performance was tested using a vector network analyzer (AV3672, China Electronics Technology Instruments Co., Ltd.) in the 8–12 GHz region (X-band). The samples, with dimensions of 22.9 × 10.2 mm^2, were tightly fixed in a copper clamp and then connected between two waveguide flanges.

3 Results and Discussion

3.1 Fabrication and Characterization of the SSG and Conductive SSG/Ni Composite Foam

The SSG/Ni composite foam was developed via a simple ultrasonic-assisted infiltration–drying approach, consisting of the preparation of SSG via high-temperature polycondensation and its subsequent introduction into the conductive Ni foam. During the high-temperature polycondensation reaction of hydroxyl silicone oil and boric acid, a large number of B-O dynamic cross-linking bonds are formed within the SSG polymer chains (Fig. 1a). These dynamic cross-linking bonds are easily broken at a low strain rate but tend to remain un-

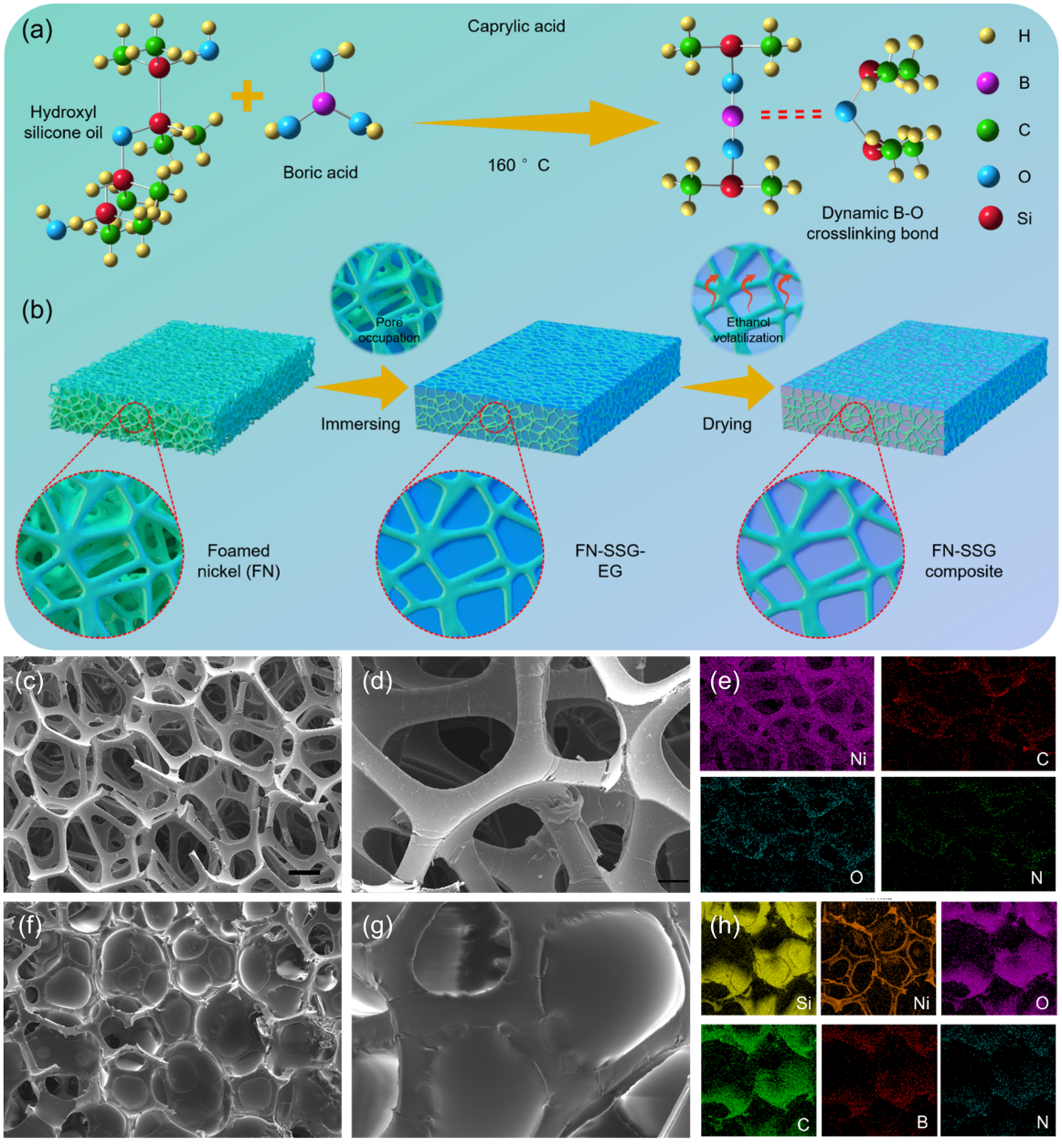


Fig. 1. (a) Preparation process of the shear stiffening gel (SSG). (b) Fabrication procedure of the SSG/Ni composite foam. (c, d) SEM images of the commercially available conductive Ni foam and (e) the corresponding energy-dispersive spectroscopy (EDS) mapping images. (f, g) SEM images of the conductive SSG/Ni composite foam and (h) the corresponding EDS mapping images.

CSTR: 32290.14.JUSTC-2025-0103
DOI: 10.52396/JUSTC-2025-0103
JUSTC, **2026**, 56(X):

altered when subjected to a high strain rate, thus exhibiting typical rate-dependent properties. The prepared SSG exhibits a plasticine-like consistency with excellent adhesion and self-healing properties, and thus can be effectively introduced into the porous Ni foam through the ultrasonic-assisted infiltration–drying method (Fig. 1b). To track the structural evolution during the preparation process, scanning electron microscopy (SEM) was used to characterize the microstructures of the pristine conductive Ni foam and the SSG/Ni composite foam. As shown in Fig. 1c and d, the pristine conductive Ni foam exhibited a distinct three-dimensional and cellular-like porous network structure, which provided sufficient space and skeletal support for the subsequent infiltration of SSG. The corresponding EDS elemental mapping indicated that the conductive Ni porous foam framework contained mainly Ni, C, O, and N (Fig. 1e). After the introduction of the SSG, the internal space of the conductive Ni porous skeleton was completely filled by the SSG, which was similar to a number of cage constructions (Fig. 1f and g). The presence of Si and B in the EDS maps further confirmed the successful introduction of SSG in the composite foam (Fig. 1h).

To verify the rate-dependent characteristics of the composite foam, compressive and tensile tests were conducted under different strain rates. For the pristine conductive Ni-coated foam, the compressive strength was essentially unaffected by the loading strain rate. As the loading frequency increased from 0.0025 Hz to 0.05 Hz, the maximum compressive strength remained essentially constant (Fig. 2a and b). When the SSG was introduced, the SSG/Ni composite foam exhibited typical rate-dependent characteristics. As the loading frequency increased from 0.0025 Hz to 0.05 Hz, the maximum compressive strength increased from 38 kPa to 118 kPa, which clearly proved that the rate-dependent behavior of the SSG/Ni composite foam originated from the shear stiffening property of the SSG (Fig. 2c and d). Furthermore, the conductive Ni-coated framework provided robust structural support for the SSG. The overall stiffness of the SSG significantly reduced the structural deformation during compression and generated an extrusion effect between the two phases, ultimately leading to an enhanced compressive strength in the SSG/Ni composite foam. Similar to the phenomena observed during compression, the tensile curves of the pristine conductive Ni-coated foam at different tensile rates essentially overlapped, whereas the SSG/Ni composite foam clearly exhibited rate-dependent performance. As the tensile rate increased from 0.4 mm/s to 4 mm/s, both the modulus and the maximum tensile strength were significantly improved, further confirming the shear stiffening characteristics (Fig. 2e and f).

3.2 Impact Resistance of the SSG/Ni Composite Foam

Owing to the rate-dependent property of the SSG and its shear stiffening effect, the developed SSG/Ni composite foam was expected to resist external impact and absorb impact energy. To systematically study the impact resistance performance of the SSG/Ni composite foams, a drop hammer impact test was conducted, as shown in Fig. 3a. In the experiments, a drop hammer with a specific mass was dropped from different heights to impact the samples. A force sensor and an acceleration sensor were used to measure the impact force and acceleration during the impact process. The original impact force–time curves of the pedestal, conductive Ni foam and SSG/Ni composite foam at different drop heights are shown in Fig. 3b–f. As the drop height increased, the impact force also increased significantly, indicating the severe damage potential of external impacts. Compared with that of the pedestal, the protective performance of the conductive Ni foam was

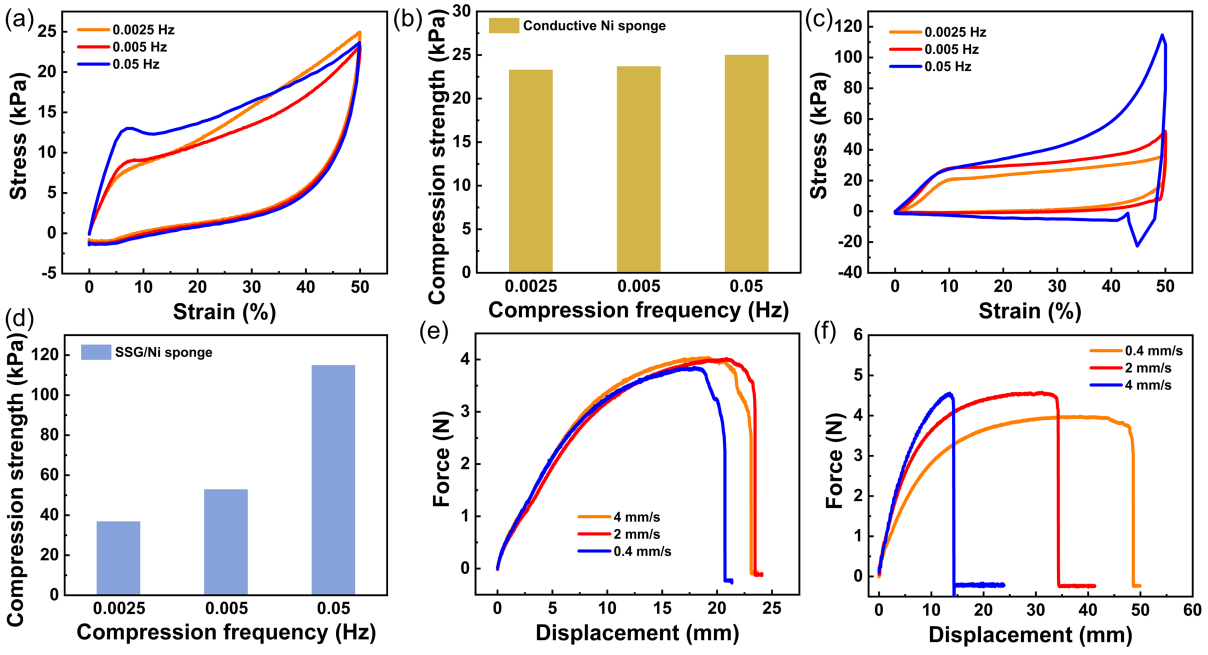


Fig. 2. (a) Force–displacement curves and (b) compression strength of the conductive Ni-coated foam under different compression frequencies. (c) Force–displacement curves and (d) compression strength of the SSG/Ni composite foam under different compression frequencies. Force–displacement curves of (e) the conductive Ni-coated foam and (f) the SSG/Ni composite foam under different tensile rates.

CSTR: 32290.14.JUSTC-2025-0103
DOI: 10.52396/JUSTC-2025-0103
JUSTC, **2026**, 56(X):

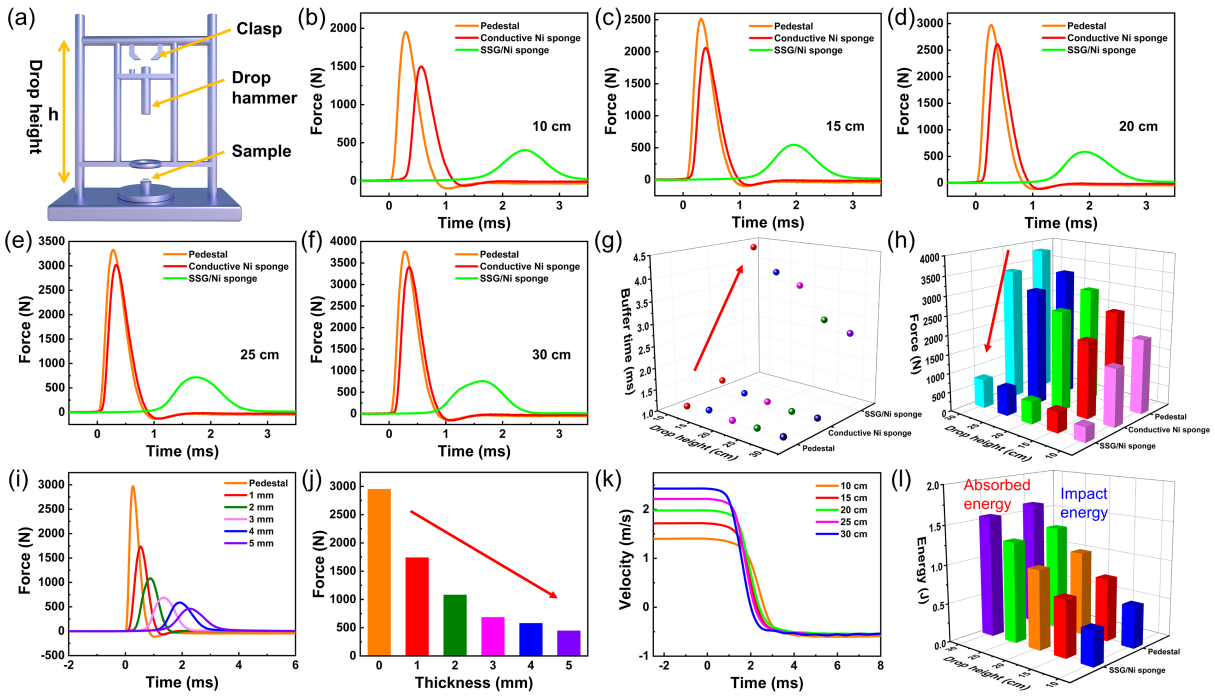


Fig. 3. (a) Schematic diagram of the drop hammer device. The impact force–time curves of the conductive Ni foam and the SSG/Ni composite foam at drop heights of (b) 10 cm, (c) 15 cm, (d) 20 cm, (e) 25 cm, and (f) 30 cm. Comparisons of (g) buffer time and (h) maximum impact force among the pedestal, conductive Ni foam and SSG/Ni composite foam. (i) The impact force–time curves of the SSG/Ni composite foam with different thicknesses and (j) the corresponding maximum impact forces. (k) Velocity–time curves of the SSG/Ni composite foam at various drop heights. (l) The impact energy and the absorbed energy at various drop heights.

limited. Upon the introduction of SSG, the impact buffering time significantly increased, and the maximum impact force notably decreased, indicating the excellent impact resistance of the SSG/Ni composite foam at different impact heights (Figs. 3g and h). Moreover, the force attenuation capacity of the SSG/Ni composite foam also increased as the thickness increased (Fig. 3i). At a thickness of 5 cm, the impact force of the SSG/Ni composite foam decreased from 3000 N to 500 N, effectively attenuating the external impact force and reducing the impact hazard (Fig. 3j). In addition, we performed a systematic investigation of the SSG loading content by preparing different samples with concentrations of 400, 600, 800, 1000, and 1200 mg/mL and evaluated their effects on impact energy absorption. The results indicate that increasing the SSG loading content enhances the impact resistance (Fig. S1). To quantitatively evaluate the energy absorption capability of the SSG/Ni composite foam, the velocity during the impact process at various drop heights was calculated. As shown in Fig. 3k, the maximum initial velocity increased as the drop height increased from 10 cm to 30 cm. Thus, the impact energy and energy absorbed by the SSG/Ni composite foam were calculated based on the Equations (1–5) in Supplementary Section 1 (Supporting Information). As shown in Fig. 3l, the SSG/Ni composite foam absorbed most of the impact energy at different drop heights. Calculations revealed that the absorption ratio of the impact energy exceeded 90%, further confirming the superior energy dissipation performance of the SSG/Ni composite foam, and demonstrating its potential as an effective impact-resistant material when subjected to external impacts. To verify the stability and durability of the impact resistance of the composite foam, we also performed repeated impact tests and performance measurements after long-term environmental exposure. The repeated impact results show that the impact resistance remains stable after ten impacts at a height of 10 cm (Fig. S2a). For the environmental aging test, the samples were stored under ambient conditions for 30 days and then subjected to ten impacts at a height of 30 cm. The initial impact resistance is largely consistent with that before aging, with only a slight decrease followed by a stable response during repeated impacts, further ensuring the reliability and applicability of the composite foam (Fig. S2b).

The superior impact resistance and energy dissipation properties endow the SSG/Ni composite foam with a considerable ability to prevent impact-induced breakage; thus, it can provide effective protection for fragile objects and miniature devices. To demonstrate its practical applicability, a commercial vase was freely dropped onto different materials from specified heights, and the entire process was captured by a high-speed video camera. When the vase was dropped directly from a 90 cm height onto the floor or the conductive Ni foam, it experienced severe breakage (Figs. 4a, b and e). However, when the vase fell onto the SSG/Ni composite foam from heights of 90 cm and 130 cm, the SSG/Ni composite foam provided significant protection for the vase, preventing any visible structural damage (Figs. 4c and f). Even when the drop height was increased to 170 cm, the vase remained completely intact under the protection of the SSG/Ni composite foam, demonstrating a remarkable impact protection capability (Fig. 4d). To further understand the impact resistance mechanism, a custom-made mechanodiscoloration approach was employed to visualize the spatial distribution of the impact force. Pressure-sensitive paper, which turns red when

CSTR: 32290.14.JUSTC-2025-0103
DOI: 10.52396/JUSTC-2025-0103
JUSTC, **2026**, 56(X):

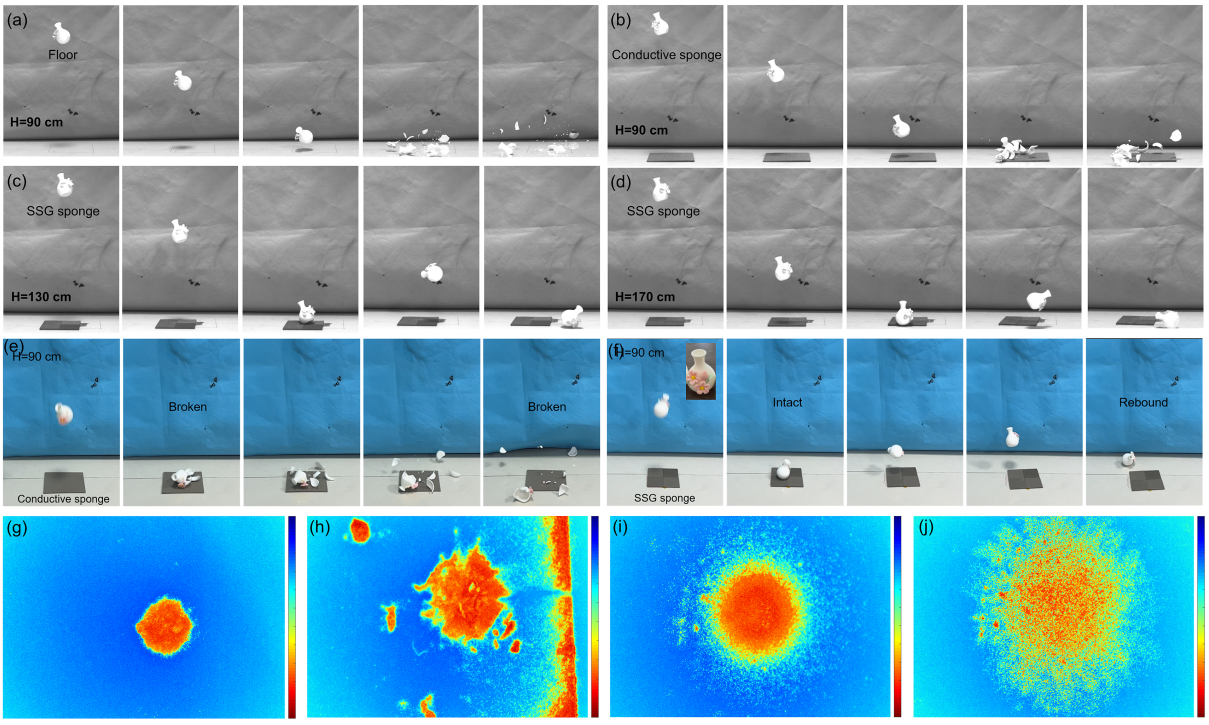


Fig. 4. High-speed photographs of the vase falling onto the (a) floor from 90 cm, (b) conductive Ni foam from 90 cm, (c) SSG/Ni composite foam from 130 cm, and (d) SSG/Ni composite foam from 170 cm. Digital photographs of the vase falling onto the (e) conductive Ni foam and (f) SSG/Ni composite foam from 90 cm. Impact force mappings using pressure-sensitive paper for (g) direct impact, (h) wood, (i) conductive Ni foam, and (j) SSG/Ni composite foam.

subjected to external mechanical impact, was used to sense the impact force, and the force distribution across different samples was reconstructed using MATLAB software. As shown in Fig. 4g, the force mapping exhibited a quasi-circular shape when directly impacted by the spherical drop hammer. The presence of wood led to mild stress transfer, causing an expansion of the contact area and a slight attenuation of the impact force (Fig. 4h). For the conductive Ni foam, the force mapping displayed a concentric circle, whose strength decreased radially, and the center value was effectively reduced compared with that of the wood (Fig. 4i). Owing to the force attenuation and energy dissipation characteristics of the SSG, the SSG/Ni composite foam also showed a similar concentric circle mapping. The intensity of its central peak was significantly reduced, and the mapping area was greatly increased, demonstrating its exceptional impact-force attenuation capacity (Fig. 4j). This spatial distribution of the impact force provided an intuitive insight into the impact resistance mechanism.

3.3 Thermal Insulation Property of the SSG/Ni Composite Foam

Considering that some thermal shocks (such as high temperatures and fires) may be encountered in practical applications, reliable thermal insulation property is crucial for materials used in extreme environments. To investigate the thermal insulation property of the SSG/Ni composite foam, various samples were placed on a hot baseplate, and the surface temperature was measured using a thermocouple (Fig. 5a). The surface temperature over time of Ecoflex, conductive Ni foam, and the SSG/Ni composite foam at different baseplate temperatures are shown in Fig. 5b–e, respectively. Here, the difference between the baseplate temperature and the surface temperature of the samples was defined as ΔT. The larger the ΔT value, the better the thermal insulation performance of the material. Compared with Ecoflex, the conductive Ni foam and the SSG/Ni composite foam both possessed larger ΔT values, thus showing superior thermal insulation performance. Since the thermal conductivity of air is lower than that of solids, the introduction of the SSG in the SSG/Ni composite foam slightly reduced its thermal insulation performance compared with that of the conductive Ni foam but still resulted in an excellent thermal insulation performance (Fig. 5f). The thermal conductivities of Ecoflex, the conductive Ni foam, and the SSG/Ni composite foam were measured as 0.20, 0.039 and 0.124 W m^{-1} K^{-1}, respectively. In addition, we performed a systematic investigation of the SSG loading content by preparing different samples with concentrations of 400, 600, 800, 1000, and 1200 mg/mL and evaluated its effect on thermal conductivity. The results indicate that increasing the SSG loading content increases the thermal conductivity (Figure S3). These findings further proved that the thermal conductivities of the conductive Ni foam and the SSG/Ni composite foam were relatively low and that the thermal insulation properties were excellent, which was consistent with the temperature test results (Fig. 5g).

To intuitively demonstrate the thermal insulation performance of the SSG/Ni composite foam, an infrared camera was used to capture the changes in the surface temperature of various samples on the baseplate at 100 °C (Fig. 5h). The surface temperature color of Ecoflex was closest to the baseplate temperature when equilibrium was reached, indicating the poorest

CSTR: 32290.14.JUSTC-2025-0103
DOI: 10.52396/JUSTC-2025-0103
JUSTC, **2026**, 56(X):

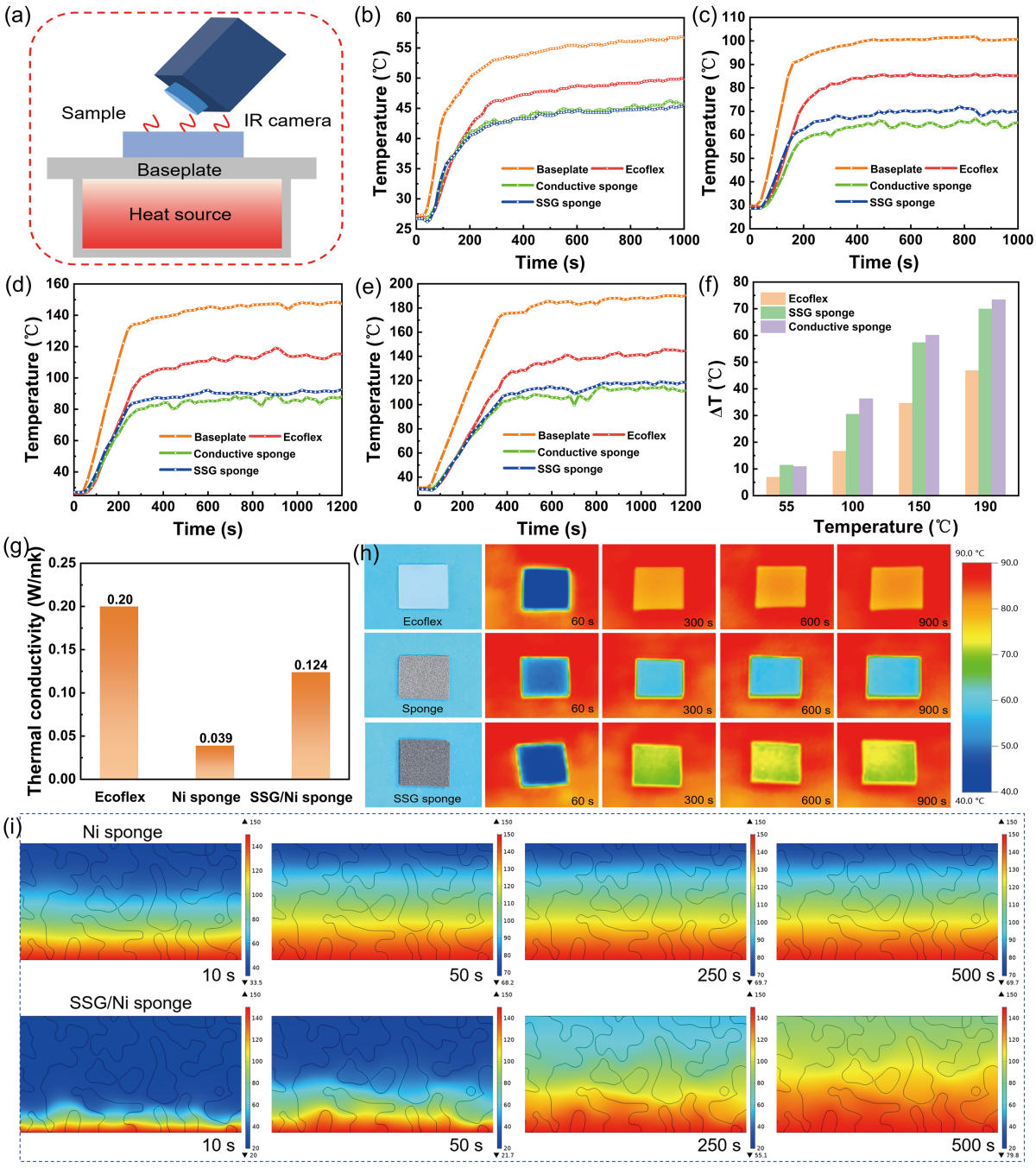


Fig. 5. (a) Schematic illustration for investigating the thermal insulation property at high temperatures. Temperature–time curves of various samples at different baseplate temperatures of (b) 50 °C, (c) 100 °C, (d) 150 °C and (e) 200 °C. (f) Difference in temperature between the surfaces of various samples and the baseplate at different baseplate temperatures. (g) Thermal conductivity of various samples. (h) Photographs and IR images of various samples over time. (i) Heat transfer process in the composite foam simulated using the finite element method.

thermal insulation capability. For the conductive Ni foam and SSG/Ni composite foam, the strong temperature color between the surface and the baseplate strongly suggested excellent thermal insulation performance. Finite element simulations using a simplified model were employed to clarify the heat conduction behavior of the conductive Ni foam and the SSG/Ni composite foam (Fig. 5i). The thermal simulation results revealed that the introduction of the SSG inhibited the conduction of heat within the conductive Ni foam during the initial stage of heating, resulting in a lower surface temperature of the SSG/Ni composite foam. When equilibrium was reached, the surface temperature of the SSG/Ni composite foam was higher than that of the conductive Ni foam. This occurred because the thermal conductivity of air is generally lower than that of the solid phase. The simulation results were consistent with the experimental results, indicating that the finite element simulation could provide reliable guidance for the structural design and performance optimization of materials.

Owing to its excellent thermal insulation property, the

CSTR: 32290.14.JUSTC-2025-0103
DOI: 10.52396/JUSTC-2025-0103
JUSTC, **2026**, 56(X):

SSG/Ni composite foam could effectively isolate external heat and provide reliable thermal protection against high temperatures. For example, two pine tree models made of paraffin (melting point: 60 °C) were placed on the Ecoflex and the SSG/Ni composite foam and then placed on a heating plate. As the temperature of the heating plate rose to 80 °C, the paraffin pine tree model placed on the Ecoflex began to melt and tilt, whereas the paraffin pine tree model placed on the SSG/Ni composite foam remained unaffected. After heating for 10 min, the paraffinized pine tree on the Ecoflex melted significantly, and a liquid pool appeared. However, the paraffin pine tree on the SSG/Ni composite foam still remained intact, indicating the excellent thermal insulation performance of the SSG/Ni composite foam, which could protect objects from high-temperature erosion (Figs. 6a–c). Interestingly, the excellent thermal insulation property of the SSG/Ni composite foam endow it with an infrared thermal camouflage capability, which enables the evasion of infrared detectors in specific environments, thereby achieving effective camouflage of the target object. To demonstrate this, a civil aircraft model was first heated to a high temperature, after which an SSG/Ni composite foam was attached to it. Although the target aircraft showed a red high-temperature signature, the color of the SSG/Ni composite foam was similar to that of the background owing to its superior thermal insulation performance; thus, the contour of the target object was successfully masked, and infrared thermal camouflage was achieved (Fig. 6d). Similarly, when the SSG/Ni composite foam was placed on a low-temperature military fighter model, the significant difference in infrared color further confirmed that it could also play an effective role in thermal camouflage for low-temperature targets (Fig. 6e). These demonstrations successfully demonstrated the potential value of the thermal insulation performance of SSG/Ni composite foams in practical applications.

3.4 Electromagnetic Shielding Performance of the SSG/Ni Composite Foam

According to previous reports, the electrical conductivity of materials is a key factor in determining their electromagnetic shielding performance. Owing to the high electrical conductivity and porous structure of metallic Ni foam, the SSG/Ni composite foam exhibits excellent electromagnetic shielding performance in the X band. Moreover, the thickness is also an important factor affecting the performance of electromagnetic shielding. As the thickness of the SSG/Ni composite foam increases from 1 mm to 5 mm, its electromagnetic shielding performance significantly improves to a maximum of 80 dB, demonstrating outstanding anti-electromagnetic interference capability (Fig. 7a). To clarify the proportion of absorption (SE_A) and reflection (SE_R) to the total electromagnetic shielding effectiveness (SE_T) and the main electromagnetic shielding mechanism, the corresponding parameters were calculated according to Equations (6–10) in Supplementary Section 2 (Supporting Information). As shown in Fig. 7b, the contribution of SE_A was always greater than that of SE_R regardless of thickness, indicating that the SSG/Ni composite foam shields electromagnetic waves mainly through internal absorption rather than mere reflection. To further explore the shielding mechanism of the SSG/Ni composite foam, the absorption coefficient (A), reflection coefficient (R), and transmission coefficient (T) were calculated, as shown in Fig. 7c. Although the R coefficient is always greater than the A coefficient regardless of thickness—indicating that a large portion of the incident waves is immediately reflected at the surface due to impedance mismatch—the higher SE_A value

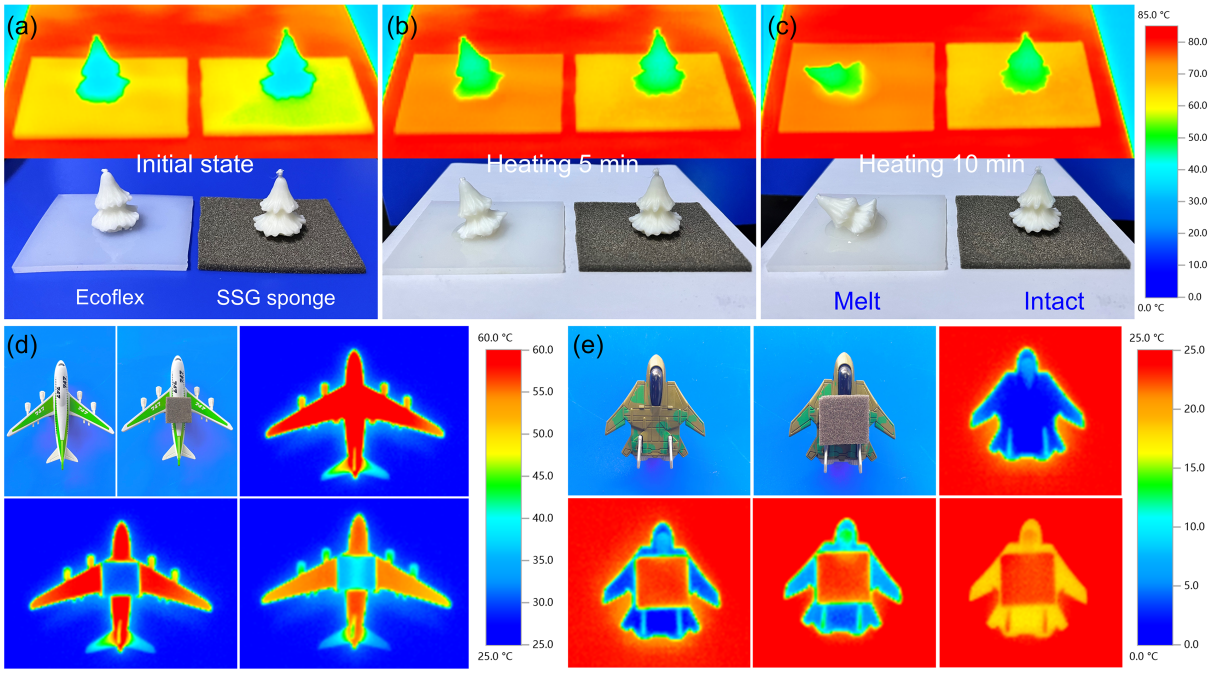


Fig. 6. (a–c) Optical and corresponding thermal infrared images showing the excellent thermal insulation property of the SSG/Ni composite foam. (d) Photographs and corresponding infrared images of a civil aircraft model covered by the SSG/Ni composite foam in a high-temperature environment. (e) Photographs and corresponding infrared images of a military fighter model covered by the SSG/Ni composite foam in a low-temperature environment.

CSTR: 32290.14.JUSTC-2025-0103
DOI: 10.52396/JUSTC-2025-0103
JUSTC, **2026**, 56(X):

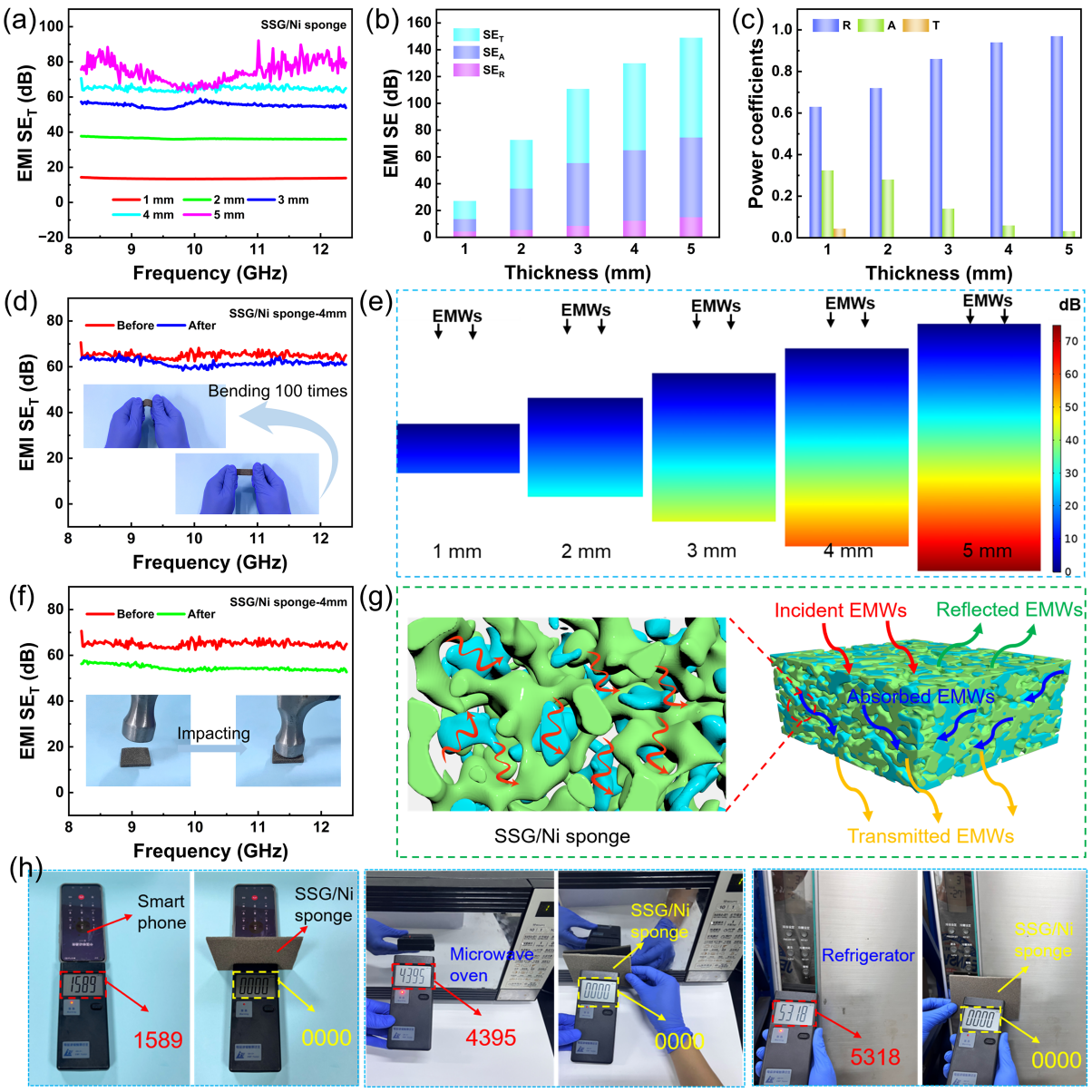


Fig. 7. (a) Electromagnetic interference shielding effectiveness; (b) average EMI SE_T, SE_A, and SE_R values; (c) corresponding R, A and T coefficients of the SSG/Ni composite foams with different thicknesses. (d) The electromagnetic shielding values of the 4 mm SSG/Ni composite foam before and after 100 bending cycles. (e) The simulated EMI SE of the SSG/Ni composite foam with different thicknesses using the finite element method. (f) The electromagnetic shielding values of the 4 mm SSG/Ni composite foam before and after impact with a hammer. (g) Schematic diagram of the electromagnetic shielding mechanism inside the SSG/Ni composite foam. (h) Demonstration showing the electromagnetic shielding performance of the SSG/Ni composite foam.

demonstrates that the overall shielding effectiveness is dominated by the absorption of the waves that successfully penetrate the material. Furthermore, the extremely low T value also indicates that most of the electromagnetic waves are effectively dissipated by the SSG/Ni composite foam, indicating its excellent shielding effectiveness. To demonstrate the superior performance of the composite foam in electromagnetic shielding, a comprehensive comparison of the EMI shielding and impact resistance between the SSG/Ni composite foam and other recently reported multifunctional foams and gels is provided in Table S1. The results indicate that compared with previously reported materials, the SSG/Ni composite foam exhibits competitive EMI shielding performance and strong impact resistance. [30–38]

In addition, the attenuation process of electromagnetic waves in the SSG/Ni composite foam was explored by FEM simulations, as shown in Fig. 7e. The thickness of the material plays a crucial role in the electromagnetic shielding effectiveness. As electromagnetic waves continuously enter the interior of the SSG/Ni composite foam, the attenuation of electromagnetic waves becomes more obvious, which further confirms the influence of thickness. To demonstrate the reliability and durability of electromagnetic shielding performance in practical applications, the influence of different working conditions on electromagnetic shielding ability was investigated. The electromagnetic shielding values of the

CSTR: 32290.14.JUSTC-2025-0103
DOI: 10.52396/JUSTC-2025-0103
JUSTC, **2026**, 56(X):

SSG/Ni composite foam before and after cyclic bending and hammer impact are shown in Figs. 7d and 7f, respectively. The electromagnetic shielding value does not decrease significantly, and the SSG/Ni composite foam still maintains good electromagnetic shielding effectiveness, thus guaranteeing the stability and reliability of its electromagnetic shielding ability. To more intuitively illustrate the shielding mechanism against electromagnetic waves, Fig. 7g shows the interaction between electromagnetic waves and the SSG/Ni composite foam. Specifically, the electromagnetic shielding mechanism of porous metal foams is a collaborative process centered on internal absorption, supplemented by multiple reflections, and is based on surface reflection. Unlike traditional dense metals, which rely mainly on single surface reflection, the three-dimensional interconnected metal network of foams transforms the surface skin effect into a volumetric interaction, providing a large effective area and tortuous paths for electromagnetic waves and causing absorption loss to dominate in the high-frequency range. The rich pore structure inside the foam simultaneously creates a large number of reflection interfaces, triggering intense scattering and ohmic losses. These scattered waves repeatedly propagate and interfere with each other in the complex pore network, resulting in the formation of a significant multiple internal reflection effect. This process does not occur independently but is achieved by prolonging the retention time and action path of electromagnetic waves within the material, repeatedly feeding the energy back to the metallic framework for dissipation as thermal energy. Surface reflection, as the first step of attenuation, has a relatively significant contribution at low frequencies. However, as the frequency increases and the wave enters the material interior, its importance diminishes relative to the combined effect of absorption and multiple reflections. Therefore, the total shielding effectiveness of porous metallic foams can be considered to be composed of initial reflection attenuation and internal absorption, thereby achieving efficient, lightweight, and absorption-based broadband shielding. To verify the application value of the electromagnetic shielding performance of the SSG/Ni composite foam in practical environments, some common electromagnetic wave radiation sources, such as mobile phones, microwave ovens, and refrigerators, were shielded for demonstration (Fig. 7h). When the SSG/Ni composite foam was not used as the shielding material, the electromagnetic radiation values of the mobile phone, microwave oven and refrigerator measured by the electromagnetic wave tester were 1589, 4395, and 5318, respectively. After the SSG/Ni composite foam was placed, the electromagnetic wave values significantly decreased to 0, demonstrating the strong shielding ability of the SSG/Ni composite foam and its promising application prospects in practical environments.

4 Conclusion

In summary, a composite foam with SSG uniformly dispersed within a conductive Ni-coated foam was developed via a facile ultrasonic-assisted infiltration approach, exhibiting excellent impact–thermal protection and high-performance electromagnetic shielding. The three-dimensional porous structure of the conductive Ni-coated foam provides a robust scaffold and structural support for the SSG, and the introduction of the SSG also enhances the mechanical properties of the foam. Owing to the shear stiffening effect of the SSG, the SSG/Ni composite foam exhibited satisfactory impact force attenuation performance and energy absorption capacity and thus effectively resisting the harmful effects of external dynamic impacts. Benefiting from the porous structure and low thermal conductivity of the Ni-coated foam, the resulting SSG/Ni composite foam presented excellent thermal insulation performance over a wide temperature range (50–200 °C), and the heat transfer process was revealed via finite element simulations. An infrared thermal camouflage experiment conducted at high temperatures further demonstrated the potential for heat insulation performance in practical environments. Finally, enabled by the excellent electrical conductivity of the porous Ni structure, the SSG/Ni composite foam could effectively reflect and absorb electromagnetic waves, achieving a maximum EMI shielding effectiveness of 80 dB at a thickness of 5 mm. This lightweight composite foam, which combines impact-thermal protection and electromagnetic radiation protection functions, is expected to become a highly promising candidate in the fields of personal protection, aerospace, and industrial construction.

Acknowledgements

Financial supports from the National Natural Science Foundation of China (Grant Nos. 12202435, 12132016, 52321003 and 12427802) and the Fundamental Research Funds for the Central Universities (Grant No. WK2090000060) are gratefully acknowledged. This study was also supported by the USTC Center for Micro and Nanoscale Research and Fabrication.

Conflict of interest

The authors declare that they have no conflicts of interest.

Biographies

Tongxin Nie received her bachelor's degree from Sun Yat-sen University (SYSU) in 2024 and is currently pursuing a master's degree at the University of Science and Technology of China (USTC). Her research focuses on designing and developing shear-stiffening smart protective systems tailored for extreme environments.

Min Sang received her Ph.D. degree from the University of Science and Technology of China (USTC) in 2021. She was subsequently a postdoctoral fellow in the CAS Key Laboratory of Mechanical Behavior and Design of Materials in Hefei. Now she is an Associate Researcher at USTC. Her research interests include the mechanical behavior design of multifunctional intelligent composite materials and their application in vibration reduction, sensing, protection, electromagnetic shielding and smart wearable devices.

Xinglong Gong received his Ph.D. degree in Mechanics from both the University of Science and Technology of China (USTC) and Saitama University in 1996. Then, he worked at Nihon Dempa Kogyo Co., Ltd., Japan. In 2003, he joined the Department of Modern Mechanics, USTC, as a Full Professor. He is currently the Chief Editor of the Chinese Journal of Experimental Mechanics, Director of the CAS Key Laboratory of Mechanical Behavior and Design of Materials. His research interests

CSTR: 32290.14.JUSTC-2025-0103
DOI: 10.52396/JUSTC-2025-0103
JUSTC, **2026**, 56(X):

comprise soft matter materials as well as their applications. He was supported by the 100-Talent Programme of the Chinese Academy of Sciences in 2003 and supported by the National Science Foundation for Distinguished Young Scholars of China in 2011.

References

[1] Qiu S, Cheng Z, Li Y, et al. Supramolecular elastomers with high strength and low toxicity are suitable for safety protection. *Chemical Engineering Journal*, **2024**, *485*: 149854.

[2] Ning H, Ren H, Wang W, et al. Impact resistance of ultra-high-performance concrete composite structures. *Materials*, **2023**, *16*: 7456.

[3] Wu L, Zhao F, Lu Z, et al. Impact energy absorption composites with shear stiffening gel-filled negative Poisson's ratio skeleton by Kirigami method. *Composite Structures*, **2022**, *298*: 116009.

[4] Cai M, Hou Y, Huang Y, et al. Impact-resistant adhesive based on the shear-stiffening effect *via* dynamic B-O linkages. *ACS Applied Materials & Interfaces*, **2024**, *16*: 57760–57768.

[5] Huang C, Wu Q, Li X, et al. Silicone bioadhesive with shear-stiffening effect: Rate-responsive adhesion behavior and wound dressing application. *Biomacromolecules*, **2024**, *25* (7): 4510–4522.

[6] Zhang Q, Xue Y, Zhao Y, et al. Shear stiffening gel-enabled twisted string for bio-inspired robot actuators. *Scientific Reports*, **2024**, *14*: 4710.

[7] Yang J, Zhao C, Lai S, et al. Hybrid additive manufacturing of shear-stiffening elastomer composites for enhanced mechanical properties and intelligent wearable applications. *Advanced Materials*, **2025**, *37*: 2419096.

[8] Zhang Z, Lin X, Lin J, et al. Cellulose supported and strengthened shear stiffening gel with enhanced impact-resistant performance. *Chemical Engineering Journal*, **2023**, *473*: 145435.

[9] Li Z, Wang S, Gong L, et al. Bioinspired flame-retardant and impact-resistant aramid composites *via* nacre-mimetic self-assembly for firefighting applications. *Advanced Materials*, **2025**, *37*: 2508606.

[10] Hu Q, Jiang J, Li Q, et al. Flame-retardant and highly thermally conductive silver nanowires/PBO nanofiber paper for high-performance electromagnetic interference shielding. *Materials Today Chemistry*, **2025**, *49*: 103048.

[11] Keshmiri N, Najmi P, Milani A S, et al. Electrospinning for electromagnetic interference shielding: Principles, challenges, and future directions. *Carbon*, **2025**, *245*: 120831.

[12] Gui J, Wang L, Li Y, et al. BN@MXene porous thermal conductive composites based on thiol-ene click chemistry and 3D printing for absorption-oriented electromagnetic shielding. *Chemical Engineering Journal*, **2025**, *522*: 167547.

[13] Wang C, Liu Y, You Q, et al. Effect of the pyrolytic carbon (PyC) content on the dielectric and electromagnetic interference shielding properties of layered SiC/PyC porous ceramics. *Ceramics International*, **2019**, *45*: 5637–5647.

[14] Li Y, Xuan X, Pan Z, et al. A robust and multifunctional conductive double-network hydrogel exhibiting self-healing, anti-freezing, antibacterial, and electromagnetic shielding properties for advanced wearable sensors and biofabrication. *Chemical Engineering Journal*, **2025**, *522*: 167264.

[15] Qiao S, Chen H, Zhao Y, et al. Bioinspired polyimide/carbon nanotube aerogels with core-radiating and omasum-like morphology toward excellent electromagnetic shielding and superior elasticity. *Advanced Materials*, **2025**, *37*: e13423.

[16] Guo H, Wan W, Deng P, et al. Gradient network structure of Fe_3O_4@MnO_2/AgNW composite films: Toward effective electromagnetic shielding. *Nanoscale*, **2025**, *17*: 20889–20902.

[17] Zhang H, Chen X, Xu S, et al. Synergistic nickel foam based composites with sulfide layers and SWCNTs for high efficiency electromagnetic shielding. *Applied Materials Today*, **2025**, *44*: 102761.

[18] Bojabady F, Kamali-Heidari E, Sahebian S. Hydrothermal synthesis of highly aligned Fe_3O_4 nanosplates on nickel foam. *Materials Chemistry and Physics*, **2023**, *305*: 127828.

[19] Li Y K, Wang W J, Cai Y J, et al. Lightweight and flexible Ni-deposited aramid fabric for electromagnetic interference shielding. *Journal of Materials Chemistry C*, **2025**, *13*: 19712–19723.

[20] Ge L, Shang S, Ma Y, et al. Overview of aerogels for thermal insulation. *ACS Applied Materials & Interfaces*, **2025**, *17* (18): 26091–26116.

[21] Li Y, Cui W, Wang X, et al. Topological polymer networks-enabled mechanically strong polyamide-imide aerogel fibers for thermal insulation in harsh environments. *ACS Applied Materials & Interfaces*, **2024**, *16*: 39993–40003.

[22] Wang Z, Zou J, Cai S, et al. Aluminum nitride-based ceramics with excellent thermal shock resistances. *Journal of the American Ceramic Society*, **2024**, *107*: 5352–5363.

[23] Qi Y, Lin K, Deng X, et al. Thermal shock behavior of Al–Y_2O_3 doped aluminum nitride ceramics. *Ceramics International*, **2024**, *50*: 39235–39242.

[24] Tiwari R, Gupta M. An investigation of biological tissue responses to thermal shock within the framework of fractional heat transfer theory. *Mechanics of Time-Dependent Materials*, **2024**, *28*: 1597–1615.

[25] Chen J, Wu Q, Wang H, et al. Modeling and analysis of ice condensation on bridge deck pavement surface based on heat transfer theory and finite element method. *Applied Thermal Engineering*, **2024**, *241*: 122344.

[26] Mai F, Deng J, Chen J, et al. Lightweight CeO_2/waterborne polyurethane foam with micronano porous structure for X-ray shielding and thermal insulation. *ACS Applied Polymer Materials*, **2025**, *7*: 10721–10729.

[27] Zhang M, Zhang Z, Zhang R, et al. Lightweight, thermal insulation, hydrophobic mycelium composites with hierarchical porous structure: Design, manufacture and applications. *Composites Part B: Engineering*, **2023**, *266*: 111003.

[28] Liu S, Wang S, Sang M, et al. Hierarchical polyimide-polyborosiloxane host-guest structure with impact resistance, acoustic and thermal insulation performance for electro-stability applications. *Chemical Engineering Journal*, **2023**, *473*: 145214.

[29] Sang M, Zhang J, Liu S, et al. Advanced MXene/shear stiffening composite-based sensor with high-performance electromagnetic interference shielding and anti-impacting bi-protection properties for smart wearable device. *Chemical Engineering Journal*, **2022**, *440*: 135869.

[30] Li S, Zhu M, Zhang Y, et al. Flexible and porous polyimide/carbon nanotube triboelectric nanogenerator for efficient electromagnetic dissipation. *Nano Energy*, **2025**, *140*: 111036.

[31] Feng J, Bai Y, Wang P, et al. Zr^{4+} and Al^{3+} coordinated cross-linked conductive collagen fibers/solvent-free polyurethane foam with ultra-low reflective electromagnetic shielding properties. *Chemical Engineering Journal*, **2024**, *499*: 156695.

[32] Liu Y, Guan Y, Li X, et al. Supercritical N_2 induced sandwich type lightweight and strong PP/CF foams with excellent electromagnetic shielding properties. *Chemical Engineering Journal*, **2024**, *501*: 157532.

[33] Liang L, Wu T, Mei X, et al. Polyetheretherketone-based foam with low reflectivity and high electromagnetic interference shielding effectiveness suitable for harsh service environments. *Chemical Engineering Journal*, **2025**, *520*: 165917.

[34] Li Z, Shen Y, Zhou Y, et al. Compressible thermoplastic polyurethane/silver nanorod foams for absorption dominant electromagnetic interference shielding. *Journal of Materials Science & Technology*, **2024**, *197*: 9–16.

[35] Wang B, Zhao Y, Xu R, et al. Cell structure design and bond-cell synergistic impact resistance response mechanism in dual network silicone rubber/PBS composite foam. *Chemical Engineering Journal*, **2025**, *524*: 169603.

[36] Fan T, Xue S S, Zhu W B, et al. Multifunctional polyurethane composite foam with outstanding anti-impact capacity for soft body armors. *ACS Applied Materials & Interfaces*, **2022**, *14* (11): 13778–13789.

[37] Cheng J, Zhang Z, Liu K, et al. Cartilage-inspired smart anti-impact gel with highly stable and tailored properties. *Cell Reports Physical Science*, **2023**, *4*: 101289.

[38] Wen H, Ma J, Jiang Y, et al. Lightweight flexible composite material with superior electromagnetic interference shielding and impact resistance properties. *Composites Communications*, **2024**, *47*: 101868.

CSTR: 32290.14.JUSTC-2025-0103
DOI: 10.52396/JUSTC-2025-0103
JUSTC, **2026**, 56(X):